Prediction of Wing Structural Mass for Transport Category Aicraft Conceptual Design

Timothy T. Takahashi[1] and Tyler Lemonds[2]
Arizona State University, Tempe, AZ

This paper describes the development of statistical semi-empirical relationships to help estimate the structural weight of wings, applicable to conventionally configured transport category aircraft design. These models are based upon a wing primary structure weight derived from an optimizing beam-element formulation. The underlying beam-element method sizes primary structure based upon "envelope" inertial and aerodynamic loads arising from maneuvering flight and hard-landing conditions. It sizes structure cognizant of tensile yield, compression yield, compression buckling of the skins and compression buckling limitations of integrally stiffened wing covers. Because our primary structural weights are based upon physical geometry we capture "real world" design effects that escape lower order physics based and purely empirical methods. Our trends differ substantially on many accounts from those "famous" wing weight regressions based upon simple strength concerns.

Nomenclature

Basic Geometry

BL	=	Butt-line (in)
FS	=	Fuselage Station (in)
WL	=	Water line (in)
x	=	Ordinate aligned with global fuselage station reference frame
y	=	Ordinate aligned with global butt-line reference frame
y'	=	Ordinate aligned with local, wing axis semi-span reference frame

Aircraft Geometry and Load Factors

Nz	=	Load factor in the z (Water Line) direction (g's)
Sref	=	Wing Planform Area (ft^2)
W	=	Weight representing Mass at 1g (lbm)
MTOW	=	Maximum Takeoff Weight (lbm)
MLW	=	Maximum Landing Weight (lbm)
t/c	=	Thickness to Chord Ratio of Wing Section (%)
b	=	Span of Wing (tip-to-tip) (ft)
c	=	Chord of Wing (ft)
t	=	Dimensional Thickness of Wing Sections (ft)
AR	=	Aspect Ratio (span / chord)
TR	=	Taper Ratio (ratio of tip-chord to center-line chord)
$\Lambda_{c/2}$	=	Mid Chord Sweep Angle (^{o})

Materials Properties

ρ	=	Material Density (lbm/in^3)
E	=	Material Elastic Modulus (lbf/in^2)
σ_{tu}	=	Material Ultimate Tensile Strength (lbf/in^2)
σ_{ty}	=	Material Tension Yield Strength (lbf/in^2)
σ_{cy}	=	Material Compression Yield Strength (lbf/in^2)
σ_{su}	=	Material Ultimate Shear Strength (lbf/in^2)

[1] Professor of Practice, Aerospace and Mechanical Engineering, School for Engineering of Matter, Transport & Energy, P.O. Box 876106, Tempe, AZ.
[2] M.S. Candidate, Aerospace and Mechanical Engineering, School for Engineering of Matter, Transport & Energy, P.O. Box 876106, Tempe, AZ. Associate Fellow AIAA.

I. Introduction

IN aircraft concept design, engineers must balance many disparate and competing interests. In order to build a vehicle that meets or exceeds its performance targets, engineers must address aerodynamics, propulsion, stability & control, maneuverability, mission performance, structural feasibility and empty weight concerns.

During traditional conceptual design, engineers typically employ empirical methods derived from "as-built" properties of historical aircraft in order to estimate the weight of the proposed structure. These algebraic methods provide a weight estimate without substantial computational effort. As a result, methods such as Raymer [1], Roskam [2], Nicolai [3], Torenbeek [4][5] and those contained within NASA's FLOPS sizing code [6] are used by academic and industrial aircraft design teams.

Purely empirical methods have many significant drawbacks. They assume that the historical aircraft used in the regression were all optimally designed; i.e. that the weights are as low as they can possibly be. They also assume that a good quality correlation can be made from this disparate basis data. Yet, empirical methods cannot account for subtle or even obvious variations in design philosophy (spar layout, rib-to-rib spacing, minimum gauges of metals).

Total wing group weight is compised of many components:

- the basic structure of the wing "torque box"
- the wing fixed leading and trailing edges
- the wing secondary structure, including doors, panels and other fittings
- wing control surfaces including ailerons, high-lift devices (leading and trailing edge), spoilers and other lift-dump and speed-brake surfaces

In our previous work [7], we extend what Professor Torenbeek once called the "weight penalty method" [4] to utilize the computational power available on a modern desktop PC. We automate the initial structural sizing of the torque-box of an aircraft wing, considering tension, shear and compressive yield criteria as well as stiffened panel and local skin buckling limitations. At this time, we have limited our scope to that of the torque box. At the present time, we do not concern ourselves with improving upon the weight estimates of secondary structure or control surfaces.

Many weight prediction methods assume that the weight of the torque box is driven solely by the tension yield limit of the structural material in the positive *Nz* load limit. For example, Torenbeek states "the amount of material in the primary structure is assumed to be affected primarily by the root bending moment due to lift." [4]

We revisit this problem with a more open mind. For example, when we address flight loads and buckling constraints in our design process, we seek to move beyond simple strength based analysis. Our method leverages many methods described in Niu [8][9]. For buckling, we consider the simple Euler-buckling problem of thin, unsupported wing skin panels as well as the overall Euler-buckling problem of a stiffened panel comprising the entire wing upper or lower "cover" structure (skin and stringers).

The idea was simple: if we can gain confidence in these methods we could produce and regress our own statistically relevant database to gain better insight into factors that impact the "as built" weight of transport category aircraft wings.

Our method is flexible enough to address wings of arbitrary outer mould line geometry lofted according to customary principles (*see* Figure 1). We may vary basic planform variables: wing-span (*b*) (tip-to-tip), wing sweep (Λ), wing taper ratio (*TR*) as well as more subtle configuration elements: the spanwise variation in wing thickness-to-chord ratio (*t/c(y)*), and planform extensions

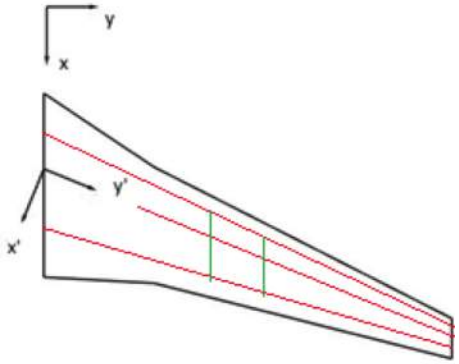

Figure 1 – Sketch of the mid-chord-sweep aligned structural coordinate system (x –y') as opposed to the global lofting coordinate system (x–y). Spar and stiffeners are called out in **red**. Rib locations are called out in green.

("yehudi's") on the leading and trailing edges. (see Figure 1). We may also trade the inter-rib spacing, the location of fuel (for inertial loads), the location of engines (for inertial relief), the location of landing gear (for both inertial relief, and for applied landing loads) (see Figure 2). We may further trade materials as we can specify structural materials of varying properties: elastic modulus (E), density (ρ), yield strength in tension (σ_{ty}), yield strength in compression (σ_{cy}) and ultimate strength in shear (σ_{su}).

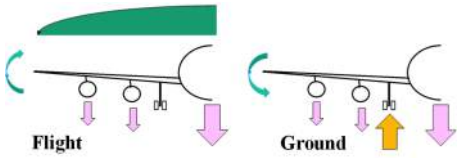

Figure 2 – Sketch of the shear and bending moment arising from wing structural and non-structural mass under flight and hard-landing loading conditions.

We gained confidence in this method by exporting our proposed geometry to *NX* (as a solid model) and *NX NASTRAN* (as a finite element model). We used *NX* to visualize our concepts, and provide a secondary check on estimated structural weight. Displacement and stress results from *NX NASTRAN* were used to validate the theoretical rule-based sizing method.

In our January 2015 conference paper [7], we provide detailed documentation, validation and initial strength based verification of our rapid design procedure.

In this paper, we will exercise the mature, developed tool to run more complex trade studies. We will document how disciplinary inputs from weight, performance, propulsion and materials groups can influence the weight and the physical design of a compliant wing. Although we search for the lowest weight structurally feasible wings, our algorithm may fail to find any wing structure sufficient to withstand the loads. Our method has the ability to report the lack of feasibility and the location and cause of such design "troubles" to designer.

II. Summary of Underlying Computational Model

The wing design structure will be predicated upon an outer-mould-line "loft" and "design loading" cases.

We will size the wing structure to a series of flight loading cases. These include: 1) flight loads based upon a maximum flight weight, *MTOW*, and a design load factor in terms of positive (NZ_{max}) and negative (NZ_{min}) g forces and 2) ground loads based upon a maximum landing weight, *MLW*, and a negative (NZ_{min}) g force applied at the landing gear frame ribs. Flight envelope load factors are specified by the FAA in 14 CFR § 25.337 [10].

Material properties are given by properties found in MIL HDBK-5J [11]. In other words,we assume isotropic properties representing bulk characteristics which include the tensile yield strength (σ_{ty}), compressive yield strength (σ_{cy}), ultimate shear strength (σ_{su}), elastic modulus (E) and density (ρ). These properties may be derated as necessary by the statutory factor-of-safety (FOS) given by the FAA in 14 CFR § 25.303 [12] (typically 1.5). Thus the derated material characteristics are:

$$\sigma_{ty}\_derated = \sigma_{ty}/FOS \quad (1)$$
$$\sigma_{cy}\_derated = \sigma_{cy}/FOS \quad (2)$$
$$\sigma_{su}\_derated = \sigma_{su}/FOS \quad (3)$$

We define the wing planform as a modified symmetrical trapezoidal shape upon which reference values are computed. The basic planform is designed in terms of a wing-tip to wing-tip overall span (b), a basic trapezoidal taper ratio (TR) which is defined as the ratio of tip to root chord of the basic trapezoid, a mid chord sweep ($\Lambda_{c/2}$) angle of the basic trapezoid as well as arbitrary spanwise chord function ($c(y)$) which allows for "yehudis," raked wingtips and other non-trapezoidal planform modifications.

If the overall wing thickness is defined in terms of an arbitrary spanwise wind referenced thickness to chord ratio ($t/c(y)$), the actual maximum thickness of the wing section may be defined in terms of the arbitrary functions $(t/c)(y)$ and $c(y)$ as:

$$t(y) = \left(\frac{t}{c}\right)(y) \cdot c(y) \quad (4)$$

Spar locations are predicated on a spanwise invariant percentage chord location based upon the fundamental trapezoidal planform. Typically the front spar is located at the 15% chord point; the rear spar at the 65% chord point. Thus, the distance between the spars is:

$$dist_{betweenspars}(y) = 0.5\, c(y) \tag{5}$$

From this geometry, the planform reference area (*Sref*) and aspect ratio (*AR*) may be defined as follows, where:

$$Sref = b \cdot \bar{c} \tag{6}$$
$$AR = b/\bar{c} \tag{7}$$
$$TR = c_{tip}/c_{root} \tag{8}$$

and

$$\bar{c} = 1/2(c_{tip} + c_{root}) \tag{9}$$

Refer again to Figure 1 (above). This formulation allows us to represent the wing in terms of a local coordinate system oriented with the mid chord sweep. In this system, the structural semi-span of the wing (that aligned with the *y'* coordinate axis) is defined as:

$$(\tfrac{b}{2})_{structural} = (\tfrac{b}{2})/\cos(\Lambda_{c/2}) \tag{10}$$

In addition to specifying the location of the front and rear spars, we may define the rib-to-rib spacing of the wing primary structure in terms of a spanwise distance, *Δy*; these too may be seen in Figure 1 (above). Thus, the presence of wing sweep alters the length of unsupported panels in the structural, *y'*, axis:

$$\Delta y' = \Delta y/\cos(\Lambda_{c/2}) \tag{11}$$

A real wing will have finite weight, which will provide inertial relief against lift induced shear and bending moment. To determine design loading, wing weight and its spanwise distribution must be taken into account (see Figure 3). We use "lumped mass" approach to define a weight distribution, *W(y)*; see Figure 3. We will oppose these inertial loads with aerodynamic loads. We assume an ideal distribution for minimum induced drag; an elliptical distribution.

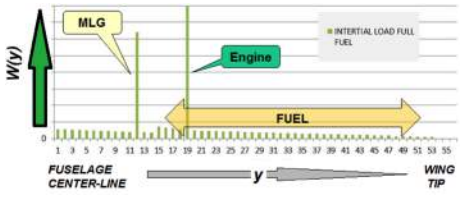

Figure 3 – Sketch of a "lumped mass" model comprising wing sturcutral and non-structural mass under a nominal 1-g loading.

$$L'(y) = C_L(y) q\, c(y) \tag{12}$$

Where $C_L(y)$ represents the section lift coefficient, C_L, as a function of the butt-line,y.

Thus, the integrated load of the wing can be found integrating this function from wing-tip to wing-tip:

$$L = \int_{-b/2}^{+b/2} L'(y)dy \tag{13}$$

Thus, the relevant shear and bending moment functions arising purely from net aerodynamic and inertial loads are:

$$\tau'(y') = \int_{y'}^{(\frac{b}{2})/\cos(\Lambda_c)} Nz\left(L'(\tilde{y}') - W'(\tilde{y}')\right)d\tilde{y}' \tag{14}$$

and

$$M'(y') = \int_{y'}^{(\frac{b}{2})/\cos(\Lambda_c)} \tau'(\tilde{y}')d\tilde{y}' \tag{15}$$

While we computed "in-plane" (y' reference axis) bending moments in equation 13, the net bending torque distribution includes secondary bending torque components induced indirectly as a result of sweep:

$$T'(y') = \int_{y'}^{(\frac{b}{2})/\cos(\Lambda_{\frac{c}{2}})} \tau'(\breve{y}')\sqrt{(1+\sin(\Lambda_{c/2})^2)}d\breve{y}' \quad (16)$$

Note that for an unswept wing ($\Lambda=0^o$), the net in-plane bending torques are identically equal to the transverse bending moment of the wing.

Neglecting buckling concerns, the wing torque box must locally and globally withstand all aerodynamically applied torques without yielding in tension or compression. This provides a means to determine the lower bound, the minimum cross sectional area of the upper or lower covers. If, for buckling reasons, additional material is needed, the stiffened panel will be heavier than needed to resist simple tension loading.

Any given bending moment (or torque) can be resolved into an individual force couple, of equal and opposite forces, *P*, acting over a distance,*d*. (refer to Figure 4)

$$T = P\,d \quad (17)$$

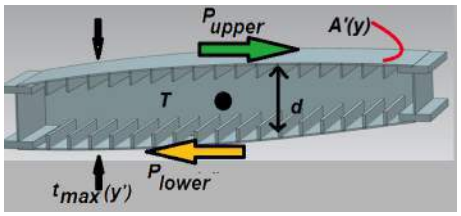

Figure 4 – Sketch resolving wing bending moment into forces along the upper and lower wing covers (comprising the spar caps, skin and any stiffeners)

Consider, a typical wing, comprising a loft approximating the classic NACA 4-digit thickness form. If the front spar caps are located at 15% chord and the rear spar caps are located at the 65% chord point, the "average" distance between upper and lower wing covers is only 70% of the magnitude of the maximum thickness of the wing. Thus, the tension and compression forces in respective lower and upper wing covers are equal to the torque divided by 0.70 of the local wing section thickness:

$$P = \frac{T}{d} \xrightarrow{yields} P(y') = +/- \frac{T(y')}{0.70\,t(y')} \quad (18)$$

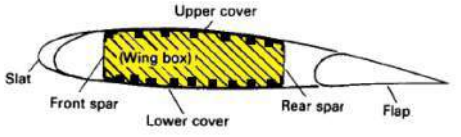

Figure 5 – Sketch resolving the torque box into spar caps, skin and any stiffeners

Thus, for a given material yield strength, σ_{ty}, the structure can withstand a tensile force proportional to the material area in upper and lower covers. Thus, the tensile strength limited cross-sectional area, *A*, of the upper or lower covers (sliced in a chord-wise plane) is:

$$A_{upper\_and\_lower\_cover} \geq P(y')/\sigma_{ty} \quad (19)$$

Substituting equation 18 into 19 results in the following relationship:

$$A_{upper\_and\_lower\_cover} \geq T(y')/(0.70\,t(y')\,\sigma_{ty}) \quad (20)$$

The relevant torque box area, $A_{upper\_and\_lower\_cover}$, for this computation comprises the following "bending resistant material." Refer to Figure 5. The spar usually looks like a modified ***I*** beam where the vertical "stroke" of the ***I*** is the spar web (typically quite thin) and the top and bottom "strokes" of the ***I*** the spar caps. The spar and spar caps may be integrally machined or built up out of smaller pieces, welded or riveted together.

Thus, when the wing resists transverse bending the spar caps and skin carry the majority of the stresses (as opposed to the spar webs) because the spar caps are furthest from the shear center of the equivalent beam.

From this, we develop a complete torque box geometry (that is to size the spar web, spar caps, skins and stiffeners) by balancing between spar caps, skins and main spar. We size the following elements, based upon the aforementioned constraints.

1. The **upper cover** (skin and stiffeners) will be sized for tensile strength from ground loads and Compressive stability (buckling) from flight loads
2. The **lower cover** (skin and stiffeners) will be sized for tensile strength from flight loads and compressive stability (buckling) from ground loads
3. The **spar caps** will be sized based upon tensile strength from ground loads traded against the overall Compressive strength and structural stability required by flight loads (the spar cap sizing can be traded off against the number and size of stiffeners)
4. The **spar web** is sized for tensile and compressive strength resisting primary wing bending as well as fuel slosh / crash loads

Our stiffened panel buckling criteria follows Niu [8], thus:

$$P_{cr\_stiffened\_panel} = \pi^2 \, E \, \left(\frac{\rho^2}{L^2}\right) A_{stiffenedpanel} \tag{21}$$

where

$$A_{stiffenedpanel} = thickness_{skin} \, dist_{spartospar} + \#_{stringers}(height_{stringer} \, thickness_{stringer}) \tag{22}$$

$$L = dist_{ribtorib} \tag{23}$$

and the radius of gyration, ρ, is described by:

$$\rho^2 = (b^2 \left(\frac{d}{b}\right)^3 \left(\frac{Ts}{t}\right))/(12 \left(1 + \left(\frac{d}{b}\right)\left(\frac{Ts}{t}\right)^2\right)\left(4 + \left(\frac{d}{b}\right)\left(\frac{Ts}{t}\right)\right)^2 \tag{24}$$

with the following relationships:

$$b = dist_{spartospar}/(\#_{stringers} + 1) \tag{25}$$
$$d = height_{stringer} \tag{26}$$
$$Ts = thickness_{stringer} \tag{27}$$
$$t = thickness_{skin} \tag{28}$$

If this critical value, *Pcr*, exceeds 150% of the actual compression force applied to the stiffened skin, the algorithm considers the net design infeasible, and moves on to examine another enumerated possibility.

Our Euler unsupported skin buckling criterion also follows a procedure recommended by Niu [8]. It employs the Euler Strip Buckling Equation using NASA factors for a strip where all edges are effectively clamped and fully supported.

$$P_{cr\_strip} = 6.3 \, E \, \left(\frac{t^3 W}{b^2}\right) \tag{29}$$

where

$$W = dist_{spartospar}/(\#_{stringers} + 1) \tag{30}$$
$$t = thickness_{skin} \tag{31}$$
$$b = dist_{ribtorib} \tag{32}$$

If this critical value, *Pcr*, exceeds 150% of the actual compression force applied to the stiffened skin, the algorithm considers the net design infeasible, and moves on to examine another enumerated possibility.

Following this procedure, our algorithm develops the minimum weight torque box geometry (sizing the spar web, spar caps, skins and stiffeners, requires us to balance loads between spar caps, skins and main spar) of a "feasible" wing.

III. Trade Study Motivation and Results

In my experience, the regressions initially published by Professor Torenbeek in his textbook "Synthesis of Subsonic Aircraft Design" [5] seem to predict weight of **large, conventionally configured** transport category aircraft **reasonably well**. These equations are also found, with only minor changes in Niu's famous "Airframe Structural Design" text [8]. At the same time, their non-physics based heritage is blindingly obvious.

Niu [8] publishes a complex equation to model the total wing weight of transport category aircraft. It estimates the structural mass of the primary wing structure, the mass of secondary structure and control surfaces as well as the non-structural mass of wing mounted subsystems.

W_{WING} estimates are expressed in terms of pounds of mass (lbm) as a function of a number of design variables:

$$W_{WING} = 0.81 \cdot \left(\frac{ULF \cdot MTOW \cdot Sref}{TCE}\right)^{0.6} \cdot \left(1 - \frac{W_{BMR}}{MTOW}\right) \cdot (1 + TR)^{0.4} \cdot \left(\frac{AR^{0.5}}{TS^{0.2} \cdot \cos(\Lambda_{c/2})^{1.2}}\right) + 3.3 \cdot S_{spoiler} + 3.28 \cdot (S_{LEflaps})^{1.13} \quad (4.6)$$

Where:

- *ULF* = Ultimate Load Factor which is the product of *Nzmax* (typically 2.5) and the design factor of safety (typically 1.5) = typically 3.75
- *MTOW* = Maximum Takeoff Weight in lbm
- *Sref* = Wing Planform Area in ft^2 ($Sref = b * (1/2)(c_{tip}+c_{root})$)
- *b* = Wing Span in ft (tip to tip)
- c_{tip} = Wing Tip Chord in ft
- c_{root} = Wing Root Chord in ft
- *TCE* = Effective Thickness Ratio ($TCE = 4/5 \, (\, t/c_{root} + t/c_{tip}) * 100$)
- *WBMR* = Weight of inertial bending-moment-relief items in lbm. This includes the weight of wing mounted engines and pylons, the weight of wing stored fuel, the weight of wing mounted landing gear.
- *TR* = Wing Taper Ratio ($TR = c_{tip} / c_{root}$)
- *AR* = Wing Aspect Ratio ($AR = b / (0.5 \, (c_{tip}+c_{root}) \,)$)
- *TS* = Design Tension Yield Stress of the Wing (baseline 70,000 lbf/in^2 for 7075-T651 aluminum)
- $\Lambda_{c/2}$ = Wing Half Chord Sweep Angle
- $S_{spoiler}$ = Spoiler Area in ft^2 for the entire wing
- $S_{LEflaps}$ = Leading Edge Flap Area in ft^2 for the entire wing

This equation substantiates the following qualitative trends: the wing grows heavier as

- the planform area increases (following a 0.6 power trend),
- the aircraft grows heavier (following a -0.6 power trend),
- the material strength increases (following a -0.2 power trend),
- the wing thickness decreases (following a -0.6 power trend),
- the aspect ratio increases (following a +0.5 power trend) ,
- the wing sweep increases (following a cosine of the sweep angle raised to the -1.2 power trend),
- the taper ratio increases (following a $(TR+1)^{0.4}$ trend), and
- the aerodynamic complexity increases (larger spoilers and more complex flaps).

Conversely, the wing is expected to grow lighter as additional bending moment relief is provided.

Through the exercise of our structural synthesis model, we will revisit the basis for these trends.

A. Basic Trades in Planform Area (holding weight constant)

In this section we will examine the effects of changing planform area, but keeping aspect ratio constant for three different sized aircraft spanning a rough order of magnitude in size: on the small end, we size the wing structure for a notional small regional jet (*MTOW*=50,000-lbm); in the middle, a small narrow body transport (*MTOW*=100,000-lbm) and at the high end, we size structure for a large twin-aisle transport (*MTOW*=400,000-lbm).

Table 1 – Planform Area Trades

	Regional Jet	Narrow-Body Airliner	Wide-Body Airliner
MTOW	50,000 – lbm	100,000 – lbm	400,000 – lbm
MLW	40,000 - lbm	80,000 - lbm	325,000 – lbm
Material	7075 (Fty=70ksi, Fsu=44ksi)	7075 (Fty=70ksi, Fsu=44ksi)	7075 (Fty=70ksi, Fsu=44ksi)
Inertial Load Limits	+2.5-g aero -3-g landing	+2.5-g aero -3-g landing	+2.5-g aero -3-g landing
Wing Planform Area	400 → 800 ft^2	700 → 1500 ft^2	2500→ 4000 ft^2
AR	8	8	8
Sweep (Λ)	30°	30°	30°
t/c	12% root → 10% tip	12% root → 10% tip	12% root → 10% tip
TR	0.279	0.279	0.279
Bending Moment Relief	2000-lbm engine at 27% semi-span	4000-lbm engine at 27% semi-span	16000-lbm engine at 27% semi-span
Rib-to-rib spacing	Optimum (typically 14-in)	Optimum (typically 14-in)	Optimum (typically 14-in)
Stiffened Skin	Optimum (typically 3-in stiffener spacing)	Optimum (typically 3-in stiffener spacing)	Optimum (typically 3-in stiffener spacing)
Spar Caps	Optimum (taper from root to tip)	Optimum (taper from root to tip)	Optimum (taper from root to tip)

The design ground rules are summarized in Table # 1, above.

The results of our wing structural synthesis tool are found in Figure 6. An interesting trend develops: in all cases, structural weight for the wing is governed by both bending and buckling rather than purely by the tensile strength needed to resist bending. As the wing planform area grows larger, holding aspect ratio constant, the span grows longer and the bending moments increase. It is no surprise that the wing becomes heavier. We find its weight growth correlating in excess of a linear change in planform area (the exponent being ~1.3 for the regional jet and narrow-body; and ~1.2 for the wide-body). This is in sharp contrast with Niu/Torenbeek who propose an exponent of 0.6.

We believe that our structural simulation is correct; see Figure 7 for a visualization of the proposed structure. Because our trade was performed at constant aspect ratio, rather than constant span, as the wings grow larger, their span increases (leading to an increase in root bending moments). Moreover, we find a curious trend. As the wing grows smaller and supports a lighter aircraft the minimum cover thickness required to resist tensile loads diminishes rapidly. Since buckling resistance scales with the c

ube of the skin thickness (refer to equation 29), halving the bending moment leads to a wing panel with one eighth the buckling resistance. It seems that lighter weight aircraft require

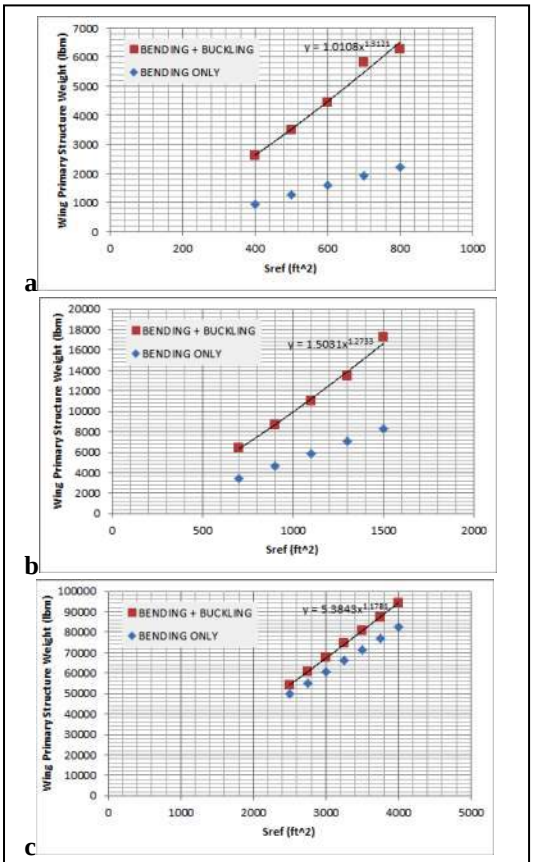

Figure 6 - Impact of changes in *Sref* on Torque Box Weight – a) 50,000-lbm, b) 100,000-lbm, c) 400,000-lbm holding *AR, TR, Λ, t/c, Nzmax* constant

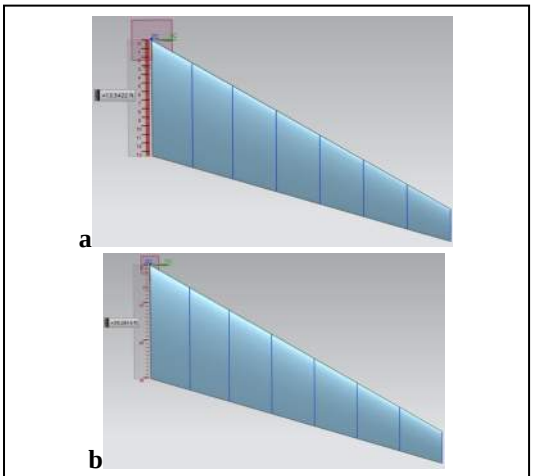

Figure 7 - Rendered Structure for a) 50,000-lbm regional jet sized wing where *Sref*=600-ft^2 b) 400,000-lbm widebody wing where *Sref* = 3000-ft^2

proportionately more attention to stiffened panel buckling concerns than do larger aircraft.

Figure 8 illuminates the root of the problem. Here we plot the spanwise distribution of required cover area for both the small and large aircraft. For the small, regional jet (Figure 8a), the entire wing structure is sized by buckling constraints. However, the buckling problem becomes more prevalent at the wing root: more than three times the cross-sectional area is required (split between spar caps, skins and stiffeners) than would be required to merely resist tension. For the large, wide-body (Figure 8b) the tension sized structure is nearly perfect. The optimizer, which selects a final design based upon discrete, common metal gauge sizes, closely tracks the minimum required cover area while it spreads the load between the spar caps, skins and stiffeners.

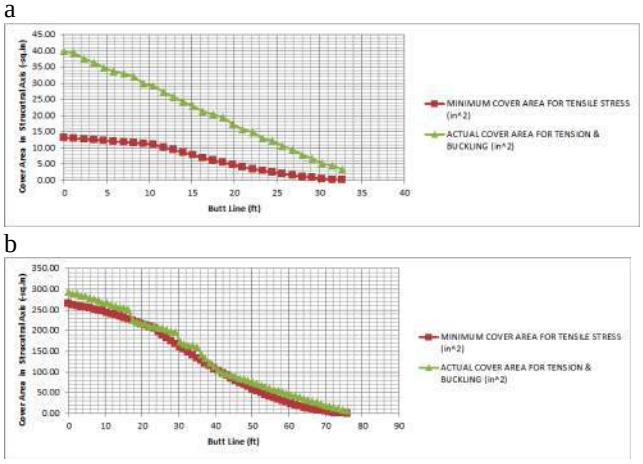

Figure 8 - Required Torque Box Area for a) 50,000-lbm regional jet sized wing where *Sref* = 600-ft^2 b) 400,000-lbm widebody wing where *Sref* = 3000-ft^2

While it may be reasonable to neglect buckling concerns when developing a simplified weight estimation method for very large aircraft, the general solution must take into consideration the weight impact of the required stiffened panel construction technique.

B. Basic Trades in Weight (holding planform area constant)

In this section we will examine the effects of changing the design maximum takeoff and maximum landing weights, but keeping wing planform area, thickness to chord ratio, taper ratio and aspect ratio constant. The design ground rules are summarized in Table # 2, overleaf.

Referring to Figure 9, the same aircraft sizing trends seen in the planform area trades remain evident: the regional jet sized aircraft has a buckling dominated structural design; the wide body aircraft has a bending strength dominated structural design; the narrow body aircraft falls in between. Within each class of airframe, the trend is qualitatively consistent with Niu / Torenbeek: as the wing planform area increases, so does its primary structural weight.

The nature of the observed correlation between weight and planform area continues to diverge greatly from prior publicaiton. Where Niu / Torenbeek suggest an exponent of 0.6; we see that trend (an ~ 0.8 power fit) occuring only with the candidate wide body airframe. For the smaller aircraft, the correlation between area and weight is much weaker (an ~ 0.2 power fit) as an increase in design maximum takeoff weight produces a smaller gain in estimated structual weight. This is due to the fact that much of the wing structure is sized by buckling concerns. Here, a small increase in the size of stiffeners dramatically increases the buckling rigidity of a stiffened panel (one that was already more than strong enough to resist the applied tensile loads).

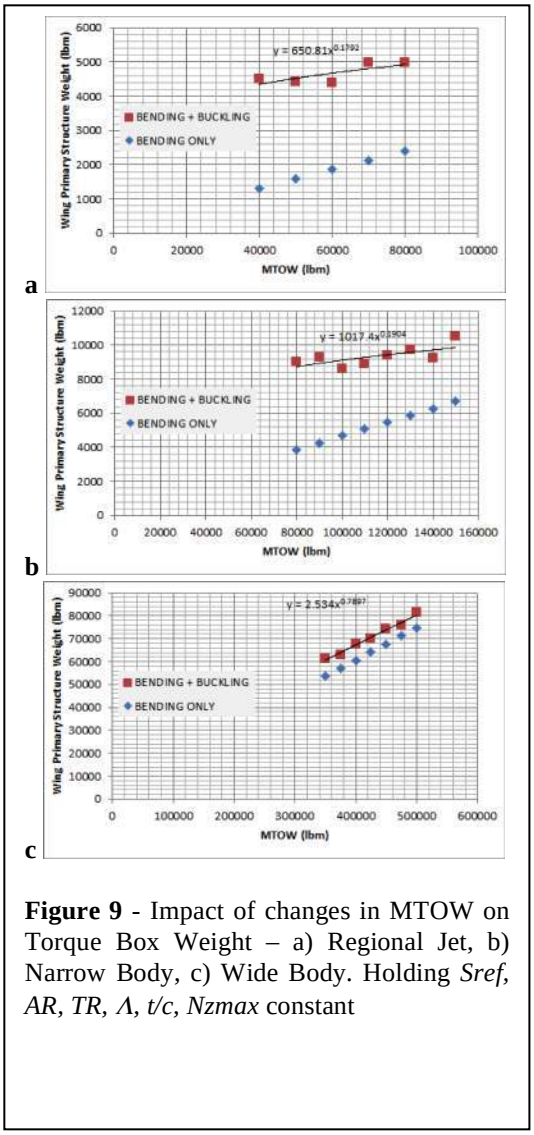

Figure 9 - Impact of changes in MTOW on Torque Box Weight – a) Regional Jet, b) Narrow Body, c) Wide Body. Holding *Sref, AR, TR, Λ, t/c, Nzmax* constant

Table 2 – MTOW Trades

	Regional Jet	Narrow Body Airliner	Wide Body Airliner
MTOW	40,000 → 80,000 lbm	80,000 → 150,000 lbm	350,000 → 500,000–lbm
MLW	80% MTOW	80% MTOW	80% MTOW
Material	7075 (Fty=72ksi, Fsu=44ksi)	7075 (Fty=72ksi, Fsu=44ksi)	7075 (Fty=72ksi, Fsu=44ksi)
Inertial Load Limits	+2.5-g aero / -3-g landing	+2.5-g aero / -3-g landing	+2.5-g aero / -3-g landing
Wing Planform Area	600 ft^2	900 ft^2	3000 ft^2
AR	8	8	8
Sweep (Λ)	30^o	30^o	30^o
t/c	12% root → 10% tip	12% root → 10% tip	12% root → 10% tip
TR	0.279	0.279	0.279
Bending Moment Relief	4% MTOW engine at 27% semi-span	4% MTOW engine at 27% semi-span	4% MTOW engine at 27% semi-span
Rib-to-rib spacing	Optimum (typically 14-in)	Optimum (typically 14-in)	Optimum (typically 14-in)
Stiffened Skin	Optimum (typically 3-in stiffener spacing)	Optimum (typically 3-in stiffener spacing)	Optimum (typically 3-in stiffener spacing)
Spar Caps	Optimum (taper from root to tip)	Optimum (taper from root to tip)	Optimum (taper from root to tip)

Table 3 – Materials Trades

	Regional Jet	Narrow Body Airliner	Wide Body Airliner
MTOW	50,000 lbm	100,000 lbm	400,000–lbm
MLW	80% MTOW	80% MTOW	80% MTOW
Material	6061/2024/7075	6061/2024/7075	6061/2024/7075
Inertial Load Limits	+2.5-g aero / -3-g landing	+2.5-g aero / -3-g landing	+2.5-g aero / -3-g landing
Wing Planform Area	600 ft^2	900 ft^2	3000 ft^2
AR	8	8	8
Sweep (Λ)	30^o	30^o	30^o
t/c	12% root → 10% tip	12% root → 10% tip	12% root → 10% tip
TR	0.279	0.279	0.279
Bending Moment Relief	4% MTOW engine at 27% semi-span	4% MTOW engine at 27% semi-span	4% MTOW engine at 27% semi-span
Stiffened Skin	Optimum (typically 3-in stiffener spacing)	Optimum (typically 3-in stiffener spacing)	Optimum (typically 3-in stiffener spacing)
Spar Caps	Optimum (taper from root to tip)	Optimum (taper from root to tip)	Optimum(taper from root to tip)

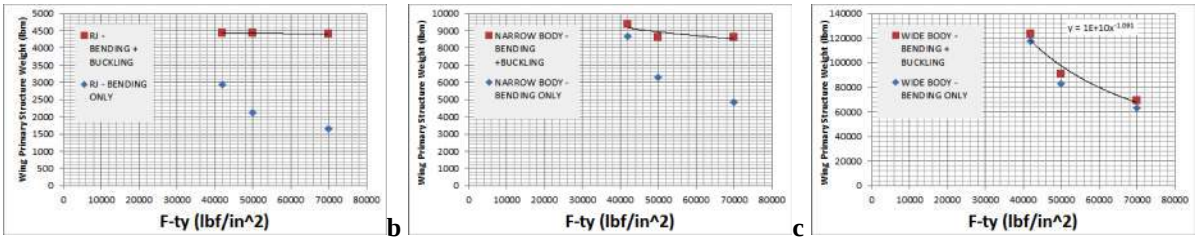

Figure 10 - Impact of changes in Materials Tensile Yield Strength on Torque Box Weight – a) Regional Jet, b) Narrow Body, c) Wide Body. Holding *Sref, AR, TR, Λ, t/c, Nzmax* constant

C. Basic Trades in Materials Properties (holding weight and planform constant)

In this section we will examine the effects of changing the design maximum takeoff and maximum landing weights, but keeping wing planform area and aspect ratio constant. The design ground rules are summarized in Table # 3, below. We will trade a wing made from 7075-T651 aluminum (*Fty*=70,000-psi, *Fcy*=67,000-psi, *Fsu*=43,000-psi) against a wing made from 2024-T62 aluminum (*Fty*=50,000-psi, *Fcy*=53,000-psi, *Fsu*=38,000-psi) or 6061-T651 aluminum (*Fty*=42,000-psi, *Fcy*=35,000-psi, *Fsu*=27,000-psi). After applying the 14 CFR § 25.303 factor of safety, the usable, derated material strengths are: 7075-T651 aluminum (*Fty*=46,667-psi, *Fcy*=44,667-psi, *Fsu*=28,667-psi) , 2024-T62 aluminum (*Fty*=33,333-psi, *Fcy*=35,333-psi, *Fsu*=25,333-psi) or 6061-T651 aluminum (*Fty*=28,000-psi, *Fcy*=23,333-psi, *Fsu*=18,000-psi).

Figure 10 demonstrates the marked difference in trending between a buckling dominated wing (the regional jet) and the strength dominated wing (the wide-body). For strength dominated wings, the higher yield strength of the 7075-T651 wing leads to a dramatic reduction in wing weight (a substitution of weak 6061 aluminum would double the structural weight). Because the difference between 6061 and 7075 alloys does not impact its elastic modulus,

there is no benefit to using the higher strength material in the buckling dominated regional jet wing. Figure 10b reveals how the 100,000-lbm class narrow-body transport occupies the transition region. Engineered to use 6061 aluminum, it is a strength dominated design; with 7075 aluminum, it is a buckling dominated design.

D. Basic Trades in Wing Thickness to Chord Ratio (holding weight and other planform parameters constant)

In this section we will examine the effects of changing the wing section thickness-to-chord ratio while keeping wing planform area, aspect ratio, sweep, taper ratio and *MTOW* constant. The design ground rules are summarized in Table # 4 (overleaf)

Figure 11 demonstrates the continued marked differences between the buckling dominated wing (the regional jet) and the strength dominated wing (the wide-body). For either wing, a reduction in wing section thickness (*t/c*) proportionally increases the tensile and compressive loads in the covers. When the wing is a strength dominated design, a doubling in tension or compression loads requires a doubling of material thickness (and, hence weight). When the wing is a buckling dominated design, smaller changes in stiffener geometry (with smaller associated changes in weight) increase the buckling rigidity of a stiffened panel to meet the higher loads. Conversely, the reduction in wing section thickness also reduces the height of the wing ribs and spar webs. Because these structural elements are sized by shear loading, their web thicknesses remain unchanged as *t/c* changes. Thus, the ribs and spar webs become lighter as *t/c* declines simply because they are physcially smaller.

The correlation between wing weight and *t/c* diverge greatly Niu / Torenbeek. They propose an universal exponent of negative-0.6. We see a similar trend (a negative ~0.7 power fit) only with the strength dominated wide body wing. For the buckling dominated regional jet wing, we see a much weaker correlation (a negative ~ 0.2 power fit) between *t/c* and structural weight.

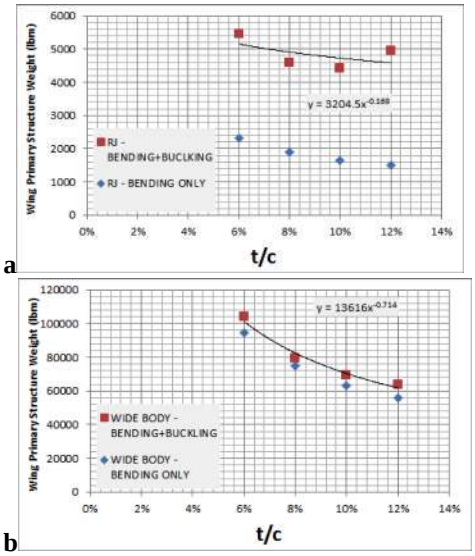

Figure 11 - Impact of changes in *t/c* on Torque Box Weight – a) Regional Jet, b) Wide Body. Holding *Sref, AR, TR, Λ, MTOW, Nzmax* constant

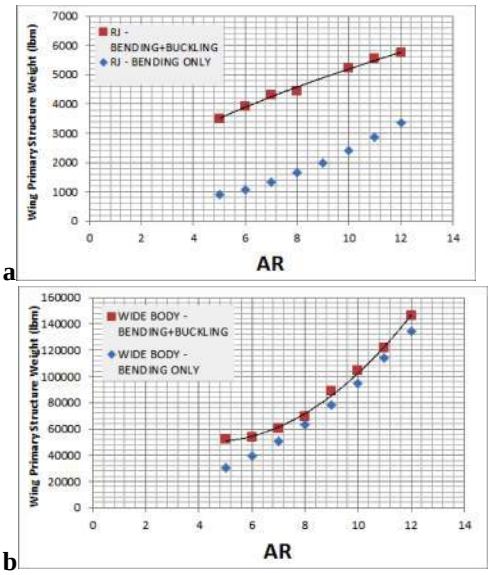

Figure 12 - Impact of changes in *AR* on Torque Box Weight – a) Regional Jet, b) Wide Body. Holding *Sref, MTOW, TR, Λ, t/c, Nzmax* constant

E. Basic Trades in Wing AR (holding planform area and weight constant)

In this section we will examine the effects of changing the wing aspect ratio (*AR*) while keeping wing planform area, thickness-to-chord ratio, sweep and *MTOW* constant. The design ground rules are summarized in Table # 5 (overleaf)

Figure 12 demonstrates the continued marked differences between the buckling dominated wing (the regional jet), the strength dominated wing (the wide-body) and the Niu / Torenbeek equations. For both wings, an increase in aspect ratio (holding area constant), leads to an increase in span, a reduction in the physical wing thickness (*t*), an increase in wing cover tension and compression forces (to react the increased bending moments arising from the longer span) and an increase in weight. However, the observed trends do not follow any sort of clear-cut power law. For the buckling dominated regional jet wing, as aspect ratio increases, the wing weight increases slower than a pure

Table 4 – *t/c* Trades

	Regional Jet	Wide Body Airliner
MTOW	50,000 lbm	400,000 -lbm
MLW	80% MTOW	80% MTOW
Material	7075 (Fty=72ksi, Fsu=44ksi)	7075 (Fty=72ksi, Fsu=44ksi)
Inertial Load Limits	+2.5-g aero / -3-g landing	+2.5-g aero / -3-g landing
Wing Planform Area	600 ft^2	3000 ft^2
AR	8	8
Sweep	30^o	30^o
t/c	8%-->14% root → 6%-->12% tip	8%-->14% root → 6%-->12% tip
TR	0.279	0.279
Bending Moment Relief	4% MTOW engine at 27% semi-span	4% MTOW engine at 27% semi-span
Rib-to-rib spacing	Optimum (typically 14-in)	Optimum (typically 14-in)
Stiffened Skin	Optimum (typically 3-in stiffener spacing)	Optimum (typically 3-in stiffener spacing)

Table 5 – *AR* Trades

	Regional Jet	Wide Body Airliner
MTOW	50,000 lbm	400,000 -lbm
MLW	80% MTOW	80% MTOW
Material	7075 (Fty=72ksi, Fsu=44ksi)	7075 (Fty=72ksi, Fsu=44ksi)
Inertial Load Limits	+2.5-g aero / -3-g landing	+2.5-g aero / -3-g landing
Wing Planform Area	600 ft^2	3000 ft^2
AR	8	8
Sweep	30^o	30^o
t/c	12% root → 10% tip	12% root → 10% tip
TR	0.279	0.279
Bending Moment Relief	4% MTOW engine at 27% semi-span	4% MTOW engine at 27% semi-span
Rib-to-rib spacing	Optimum (typically 14-in)	Optimum (typically 14-in)
Stiffened Skin	Optimum (typically 3-in stiffener spacing)	Optimum (typically 3-in stiffener spacing)

Table 6 – *TR* Trades

	Regional Jet	Wide Body Airliner
MTOW	50,000 lbm	400,000 -lbm
MLW	80% MTOW	80% MTOW
Material	7075 (Fty=72ksi, Fsu=44ksi)	7075 (Fty=72ksi, Fsu=44ksi)
Inertial Load Limits	+2.5-g aero / -3-g landing	+2.5-g aero / -3-g landing
Wing Planform Area	600 ft^2	3000 ft^2
AR	8	8
Sweep	30^o	30^o
t/c	12% root → 10%-tip	12% root → 10% tip
TR	0.279	0.279
Bending Moment Relief	4% MTOW engine at 27% semi-span	4% MTOW engine at 27% semi-span
Rib-to-rib spacing	Optimum (typically 14-in)	Optimum (typically 14-in)
Stiffened Skin	Optimum (typically 3-in stiffener spacing)	Optimum (typically 3-in stiffener spacing)

Table 7 – Sweep Trades

	Regional Jet	Wide Body Airliner
MTOW	50,000 lbm	400,000 -lbm
MLW	80% MTOW	80% MTOW
Material	7075 (Fty=72ksi, Fsu=44ksi)	7075 (Fty=72ksi, Fsu=44ksi)
Inertial Load Limits	+2.5-g aero / -3-g landing	+2.5-g aero / -3-g landing
Wing Planform Area	600 ft^2	3000 ft^2
AR	8	8
Sweep	$0 \rightarrow 40^o$	$0 \rightarrow 40^o$
t/c	12% root → 10% tip	12% root → 10% tip
TR	0.279	0.279
Bending Moment Relief	4% MTOW engine at 27% semi-span	4% MTOW engine at 27% semi-span
Rib-to-rib spacing	Optimum (typically 14-in)	Optimum (typically 14-in)
Stiffened Skin	Optimum (typically 3-in stiffener spacing)	Optimum (typically 3-in stiffener spacing)

bending model would predict. For the strength dominated wide-body design, the wing weight behaves as expected. However, the observed trends have an effective exponent equal to or greater than 1. This is very different from the proposed ½ power trend found in the Niu / Torenbeek equation.

F. Basic Trades in Wing TR (holding planform area and weight constant)

In this section we will examine the effects of changing the wing's taper ratio (*TR*) while keeping wing planform area, aspect ratio, sweep, thickness-to-chord ratio and MTOW constant. The design ground rules are summarized in Table # 6 (above).

Figure 13 demonstrates certain similarites between the buckling dominated wing (the regional jet) and the strength dominated wing (the wide-body) and that proposed by Niu / Torenbeek. For our solutions, a change in taper ratio (without a change in ellipitical span loading) does not change the bending moment distribution. As $TR \rightarrow 0$, the wing's root chord grows longer and the tip chord grows shorter. Some portions of the wing become heavier, and others lighter. Our simulations show this to be a "wash" – with no clearcut trend forming.

Niu / Torenbeek propose a relationship based upon a factor of $(1+TR)^{0.4}$; this trend is rendered as Figure 14. It does not look qualitatively different from the effects we obtained through structural synthesis. We believe that this element of the Niu / Torenbeek wing weight relationship is reasonable.

G. Basic Trades in Wing Sweep (holding planform area and thickness constant)

In this section we examine the effects of changing the wing sweep while keeping wing planform area, aspect ratio, thickness-to-chord ratio, taper ratio and *MTOW* constant. The design ground rules are summarized in Table # 7 (above).

Figure 15 demonstrates the impact of wing sweep upon the buckling dominated wing (the regional jet) and the strength dominated wing (the wide-body) and that proposed by Niu / Torenbeek. For our solutions, a change in wing sweep (holding aspect ratio constant) increases the physical length of the equivalent cantilevered beam (this grows inversely proportional to the cosine of the sweep angle). Because there is no change in the ellipitical span loading, the effective bending torque's increase proportional to the increase in length of the beam. For both wings, weight increases noticably as sweep exceeds 25^{o}.

Niu / Torenbeek propose a relationship based upon a factor of: $\cos(\Lambda)^{-1.2}$. In Figure 16 (overleaf), we plot the same weights as shown in Figure 15, but have changed the x-axis from sweep (Λ) to $\cos(\Lambda)^{-1.2}$. Both the regional jet weight data and the wide body data fall on straight lines when plotted in this manner even though the regional jet wing weights do not otherwise closely

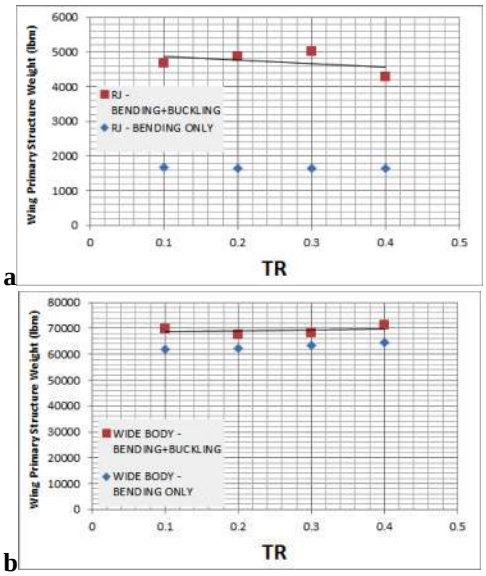

Figure 13 - Impact of changes in *TR* on Torque Box Weight – a) Regional Jet, b) Wide Body.

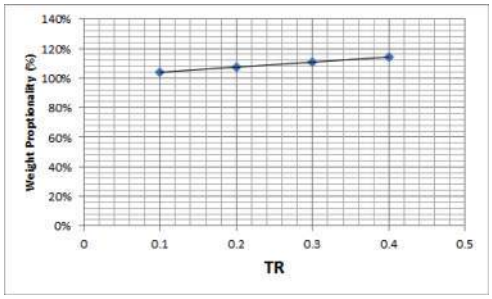

Figure 14 -Torenbeek/Niu Taper Ratio Proportionality Factor

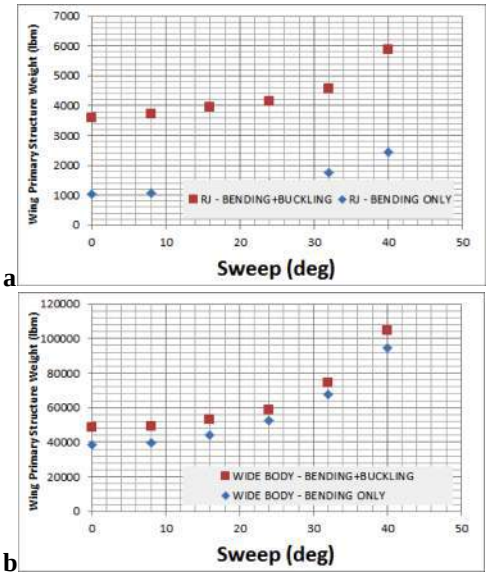

Figure 15 - Impact of changes in Sweep on Torque Box Weight – a) Regional Jet, b) Wide Body. *Sref, MTOW, AR, TR, t/c, Nzmax* held constant

correlate with the Torenbeek's strength dominated analysis. Thus, we believe that the sweep correction element of the Niu / Torenbeek wing weight relationship is reasonable and broadly applicable.

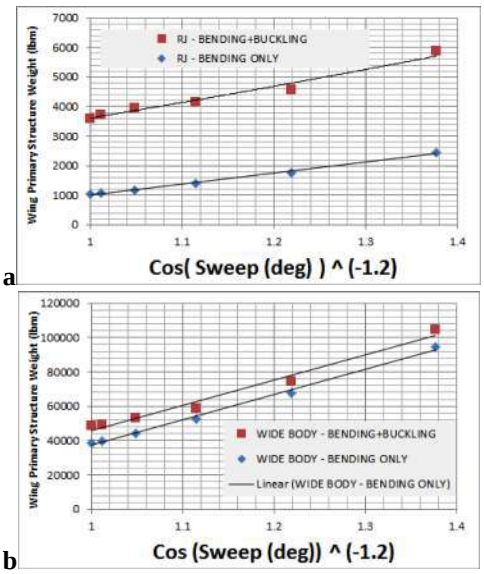

a

b

Figure 15 - Wing Structural Weight Trades – Impact of changes in Sweep on Torque Box Weight – a) Regional Jet, b) Wide Body. Holding Sref, AR, TR, Λ, t/c, Nzmax constant (cos(sweep)^-1.2) trend verification

IV. Discussion Regarding Buckling

We employed the same method as detailed in our January 2015 paper [7] to generate finite element models of the various wing geometries described by Tables 4-7. Linear buckling analysis uses the *NASTRAN* SOLN 105 solver in *NX CAE* [13]. Performing a simulation in this solver requires two subcases: buckling loads and buckling method. In the buckling loads subcase the constraints and loads are applied at the rib-skin intersection points (except for the root rib) and at a chordwise location midway between the front and aft spars, on the lower wing skin.

When the simulation is begun, the buckling loads subcase *NASTRAN* solves as a typical linear static analysis. It generates displacements, stresses, and corresponding surface contours. Next, *NASTRAN* computes the buckling method where stress and strain results are produced for ten different buckling modes, each corresponding to a specific eigenvalue. The first buckling mode is the most important one for physical relevance; it indicates where buckling will first occur.

The eigenvalue that corresponds with this first buckling mode indicates the magnitude of the load that will cause local buckling. More specifically, multiplying the eigenvalue by the load that was applied at and caused the local buckling will yield the critical load of that geometry. With this in mind, all loads used in the linear buckling analysis were input as unit loads (1 lbf) so that the first buckling mode eigenvalue effectively describes the magnitude of the critical buckling load in lbf.

This method of linear buckling analysis was found to only be effective to examine local geometries of the wing structure. If unit loads are applied at every rib-skin intersection as they are in the linear static analysis validation, the first location of buckling failure will always occur at the most outboard rib as this is the where the thinnest element thickness is allocated. However, this scenario did serve as a type of validation as it confirmed that the thicknesses were properly allocated since it would be expected that the thinnest sheet metal would buckle first and the magnitude of the eigenvenvalue confirmed that thickness of even the most outboard rib was correctly generated.

Here, we verify our methods through the study of a "Mock B737"-sized aircraft wing as discussed in our January 2015 paper [7]. This structure was synthesized to the following requirements:

1. Maximum Take-Off Weight (116,000-lbm) used to calculate the $+Nz_{max}$ envelope load case (wingtips bend upwards)
2. Maximum Landing Weight (92,800-lbm) used to calculate the $-Nz_{min}$ envelope load case (based on a 3-g hard landing) (wingtips bend downwards)
3. Design Nz_{max}=+2.5 g's
4. Design Nz_{min}=-1.0 g (flight), -3.0 g's (ground)
5. Wing Span, b=93-ft (tip-to-tip)
6. $Sref$ = 980-ft^2
7. Taper Ratio, TR = 0.279
8. Aspect Ratio, AR = 8.825
9. Wing Chord

a. Actual Centerline Chord, 19-ft
b. Trapezoidal Planform Centerline Chord, C_0 = 16.5-ft
c. Trapezoidal Planform Tip Chord, C_t = 4.6-ft

10. Thickness to Chord Ratio, *t/c(y)* = 14% at root, tapering to 10% at 30% semi-span and holding this value to the tip
11. Distance between spars = 50% of trapezoidal planform
    a. Front Spar @ 15% chord of trapezoidal planform
    b. Rear Spar @ 65% chord of trapezoidal planform
12. Rib to Rib Spacing, 18-in BL in overall aircraft coordinate frame
13. Wing Bending Moment Relief
    a. Overall Structure: 12% of overall aircraft maximum take-off weight
    b. Fuel Load: 49,000-lbm overall (24,500-lbm per semi-span) distributed between 10% and 80% semi-span
    c. Engine & Pylon: 4300-lbm at 26% semispan
    d. Landing Gear @ 15% semispan
14. Primary Structural Material: 6061 Aluminum

To better document the wing's resistance to buckling, we must examine the structure at a local rather than global perspective.

Our basic synthesized wing structure, elemental stresses and displacements are found in Figure 16, below. Being a buckling dominated design, the von Mises elemental stresses never exceed the 28,000-psi derated material limit at the design load condition (Nz_{max} at MTOW). To decide if this wing is not overly sturdy, we must examine its resistance to buckling at a local area.

The first local area of interest to be examined was the rib-skin intersection that experienced the greatest load which would be where the engine is located. One single unit load was applied at this location where the magnitude dicated by the spreadsheet was of course ignored but the direction of it was not. Figures 17 through 19 (overleaf) illustrate such a result from this simulation where the eigenvalue of the first buckling mode indicates a critical buckling load of -8521 lb while the spreadsheet only applies a -6277 lbf load at that location (buckling factor-of-safety of 1.36). Given the requirements for a 1.5 factor-of-safety for wing ultimate strength (i.e. collapse) rather than a prescription against incipient buckling above the design loads, we believe that these results validate that our current method has appropriately captured the need to simultaneously design for strength and structural stability.

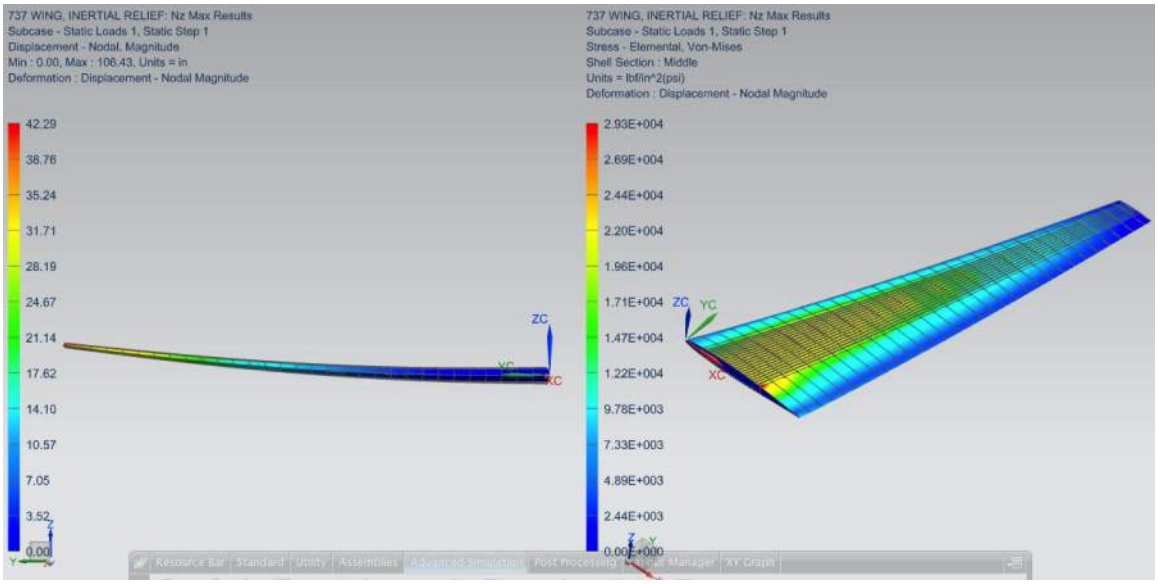

Figure 16– von Mises elemental stress and displacement surface contours for the mock 737 wing

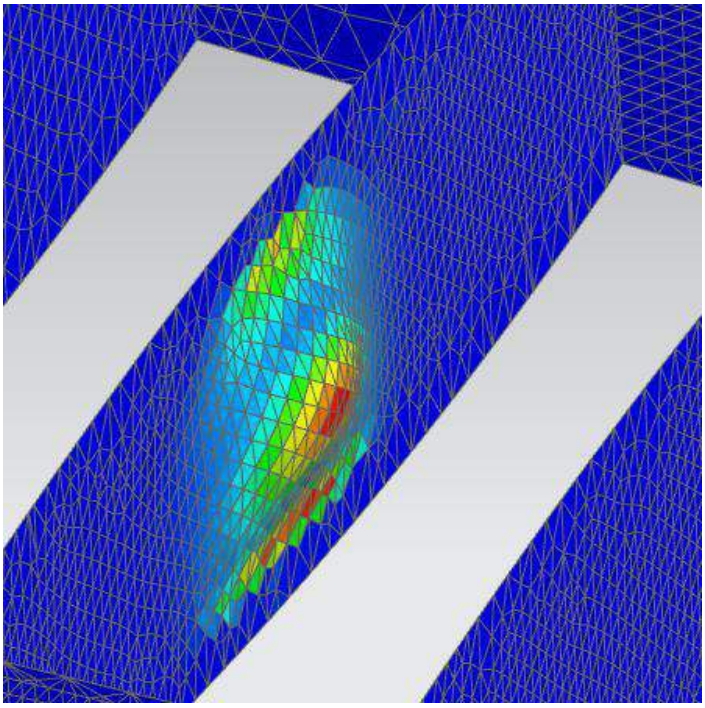

Figure 17 - Zoomed in view of one side of a buckled rib on the mock 737 wing. Design Nz loads applied at the maximum takeoff weight. Note: the deformation scale has been doubled for better visualization

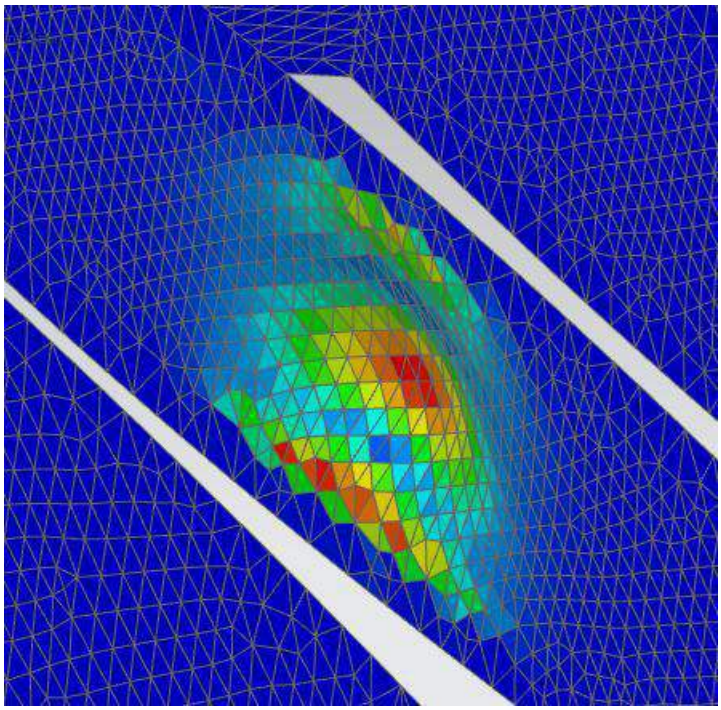

Figure 18- Zoomed in view of the other sie of the buckled rib of the mock 737 wing. Design Nz loads applied at the maximum takeoff weight. Note: the deformation scale has been doubled for better visualization.

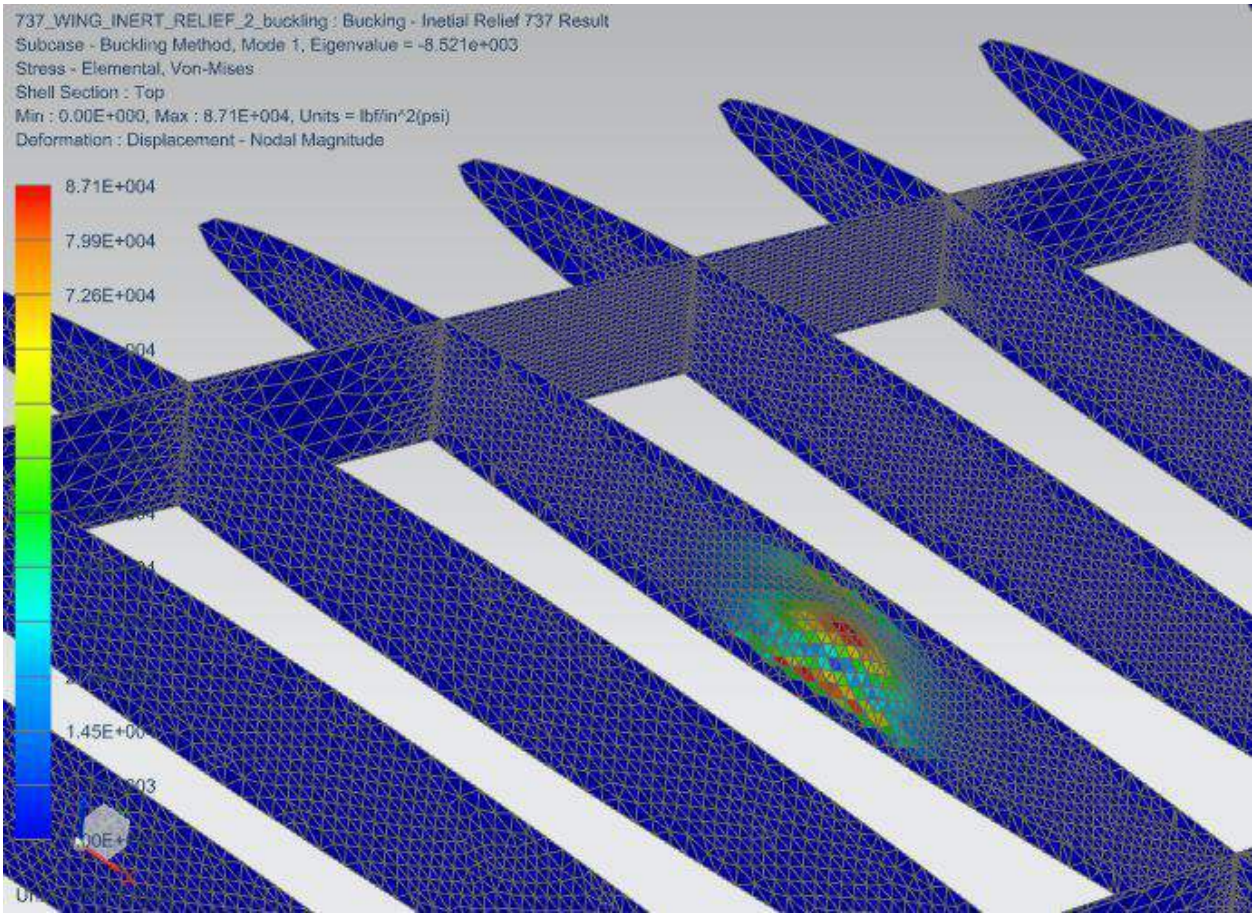

Figure 19 - Zoomed out view of rib shown in Figures 17 and 18 with the corresponding Eigenvalue show in top left corner as well as stress contour legend

The second local area of interest, which is especially important for overall structural integrity, comprises the upper wing surface stiffened skin pnaels. These are most prone to buckling as they are under compression during the Nz_{max} scenario. Here we perform a linear static analysis simulation with the entire wing (refer back to Figure 16) and all the loads at proper magnitudes in their usual bottom rib-skin intersection points. We then export the magnitude in inches and Cartesian global coordinates of all the nodal deformations from this whole-wing analysis. We further isolate a single upper stiffened wing panel of interest in the solid model and export it as a separate idealized FEM part file. We stitch the bottom edges of the stiffeners to the wing skin surface so that the stiffener-skin interfaces will share meshing nodes.

We remesh the wing skin panels and stiffeners at a very fine level. For instance, the wing skin shown in Figures 20 through 22 (overleaf) have been remeshed with element sizes of 0.1 in^2. This is compared to the NX-recommended mesh size of about 2 in^2 for said panel that we used in the previous whole-wing static analysis. All of the outside edges of the stiffened panel are selected to have enforced displacement constraints applied (see Figure 20). The enforced displacements are imported from the same file of displacements exported earlier from the whole-wing static linear static analysis model. Since the panel was isolated from the same whole-wing model used in the static analysis, the proper displacements at the proper locations are automatically applied. This operation fully constrains the local panel model.

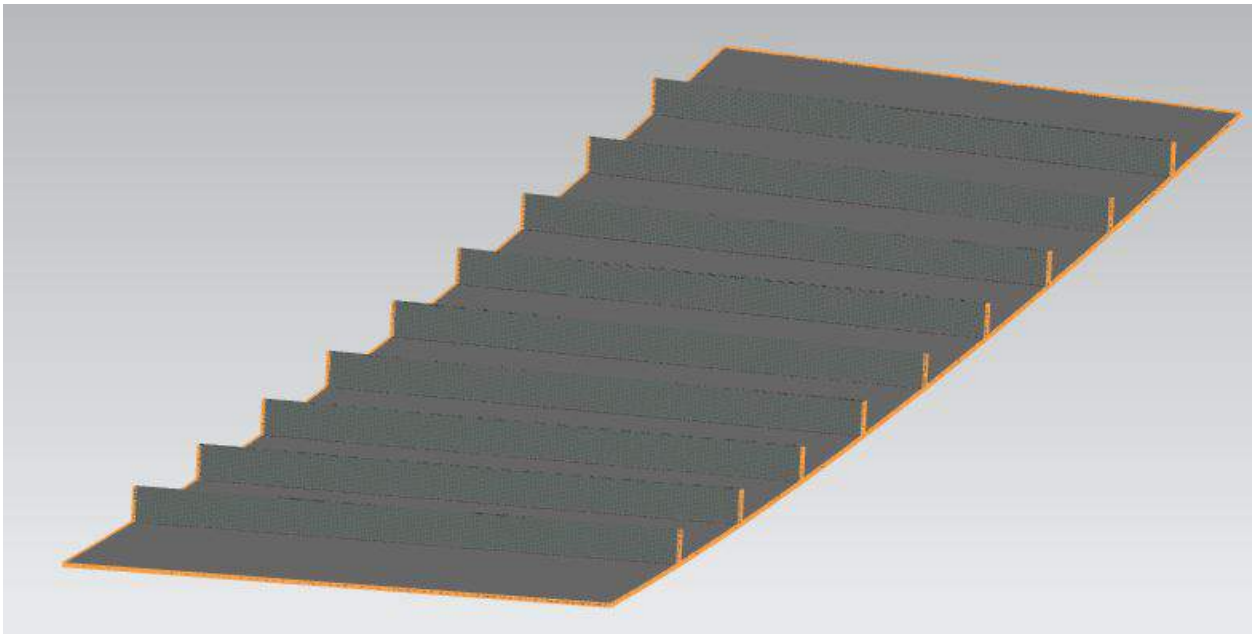

Figure 20 - Single upper wing skin panel mesh model with edges highlighted where enforced displacement constraints are applied.

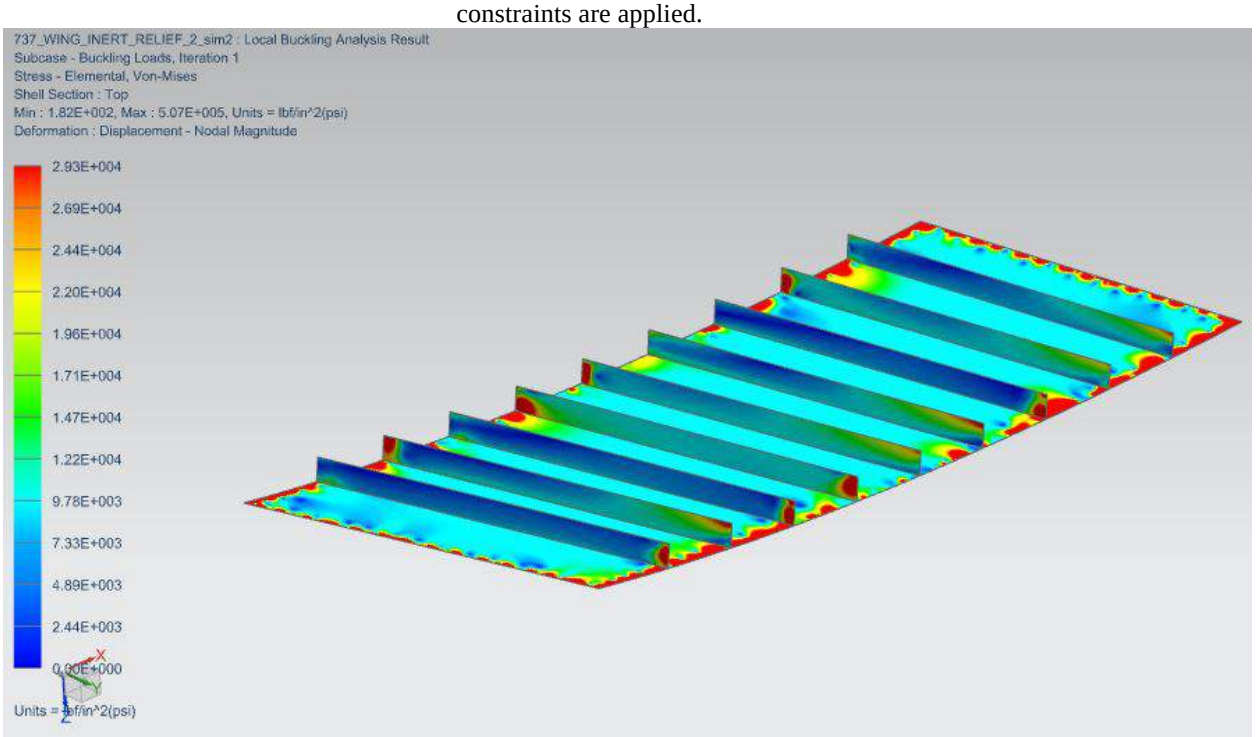

Figure 21 - Stress surface contour plot of single upper stiffened wing skin panel from linear static load analysis (note that it is "flipped upside down" as positive Z is pointing downwards)

We then ran linear buckling analysis on this sub model. One such wing panel evaluated with this method was the ninth (measured from the root) upper stiffened panel from the wing tip of the mock 737 wing. The wing synthesis alogirthm develops this panel comprising stiffeners with shell element thickness of 0.5625 inches on top of a 0.375 inch thick wing skin panels. Figure 20 (above) displays the stresses experienced by the panel when running a linear static analysis run. While there are hotspots on the edges of the panel, the majority of the model is well under the derated critical stress value of ~28,000-psi. The outside hotspots can be expected as the enforced displacments are applied directly to the perimeter edges. With such a fine mesh this method of stress distribution is bound to cause such hotspots although these higher values are quickly redistributed throughout the panel. This analysis deomonstrates that the material characteristics in tension and shear are sutiable for application in the synthesized geometry.

Figures 22 and 23 (overleaf) showcase the stress and displacements, respectively, experienced by the panel when this first buckling failure occurs. The linear buckling analysis produced a first buckling mode failure with an eigenvalue of 1.879. This essentially means that the stresses/displacements experienced at the isolated panel due to the whole-wing Nz Max scenario have a buckling safety factor of 1.879 before buckling will occur. We believe that this analysis successfully validates our design process; that the wing skin panel had its stiffener and skin thicknesses correctly allocated to avoid compression surface buckling under the design loads (Nz_{max} @ *MTOW*), and that compression surface buckling onset is likely to occur at the certification loading conditions (1.5 * Nz_{max} @ *MTOW*).

We compare these results against the spirit of the wording in 14 CFR § 25.305: that "the structure must be able to support limit loads without detrimental permanent deformation." [14] No yielding in tension or shear is prediction. Furthermore, the structure is "able to support ultimate loads without failure … [where] the deformations involved are fully accounted for in the analysis." [14]. Between the 1.36 predicted factor-of-safety regarding buckling of a critical rib and the 1.879 predicted factor-of-safety regarding buckling of a critical upper surface stiffened panel, we believe that the global weight trends predicted by our synthesis procedure are reasonable.

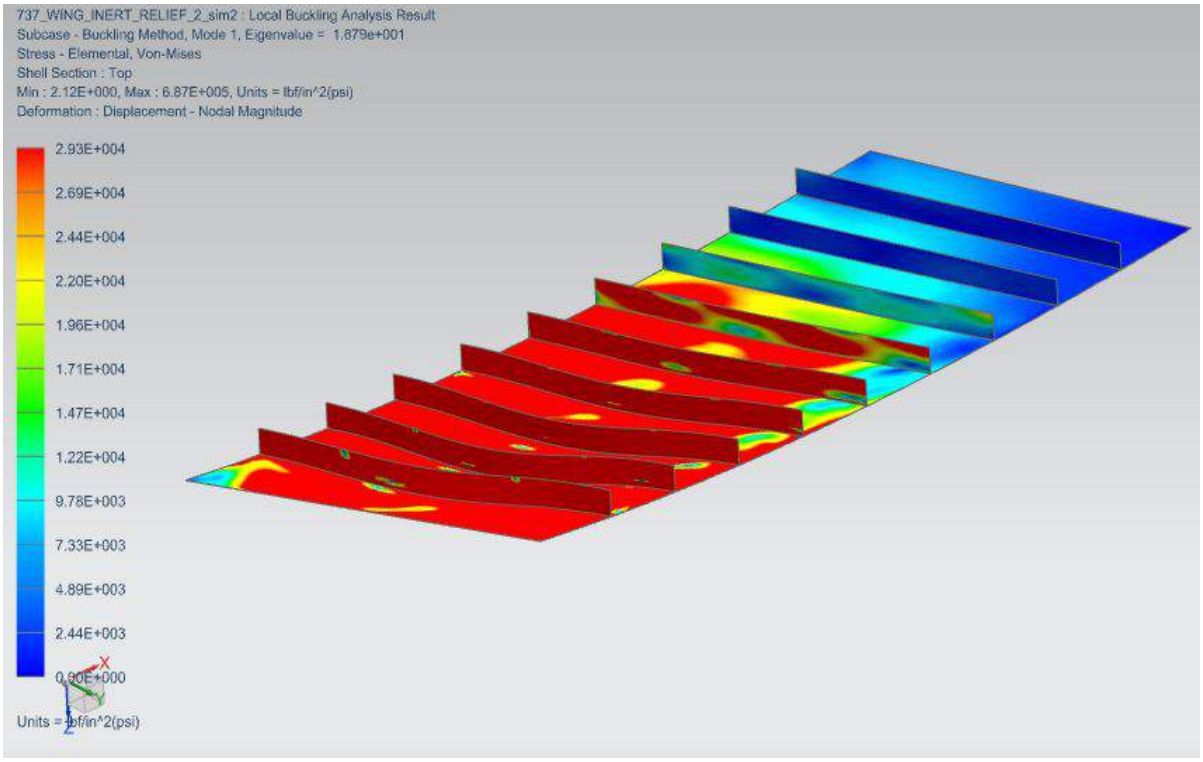

Figure 22 - Surface stress contour plot of isolated wing skin panel at first buckling mode failure.

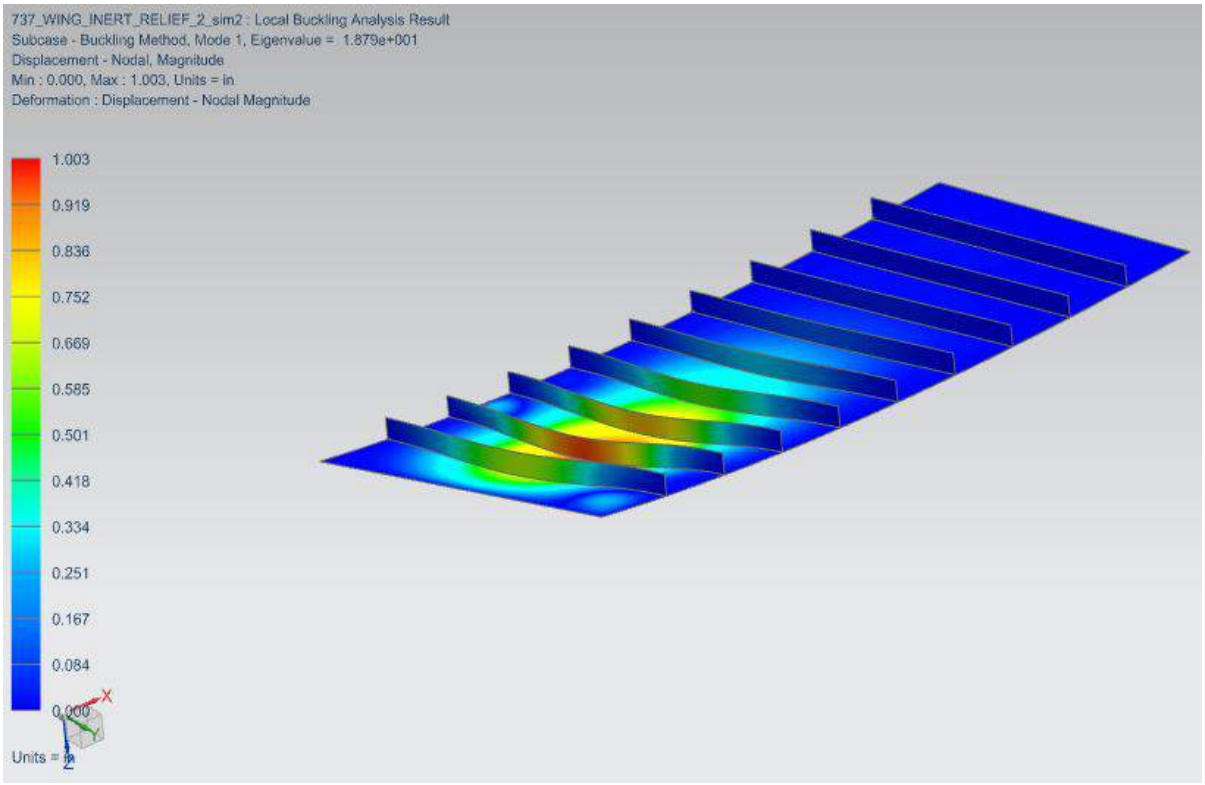

Figure 23: Displacements surface contour plot of isolated wing skin panel at first buckling failure mode.

This local method of evaluating the most buckling-prone components of the wing—stiffened wing skin panels in compression—successfully provides high fidelity validation that buckling will not occur. While some extra time is needed to isolate and prepare specific panels of the wing, an efficient strategy would be to look at panels with a combination of high compression stresses and small thicknesses relative to the rest of the wing. However, if there was sufficient confidence in the structural integrity of the wing under static linear analysis, another approach would be only model, mesh, and analyze a set of wing skin panels where high compressive loads are expected. This method in combination with isolating and evaluating highly loaded ribs for buckling modes serve as successful validation of the geometry algorithm.

V. Conclusions

To conclude, we get the same trends, but sometimes we get very different "exponents" than Torenbeek did. We think this is because wings are buckling driven design problems. Our high fidelity FEM based validation procedure indicates that this structural synthesis algorithm produces reasonably good quality initial designs. They are neither overly strong nor unacceptably weak in tension or shear. Despite their increased weight (as opposed to a purely strength based design), they are neither overly susceptible to buckling or collapse nor excessively reinforced.

The trends shown here are eye opening, as they demonstrate that a traditional strength based model of wing structural weight, while applicable to very large (i.e. *MTOW*>200,000-lbm) aircraft is both quantitatively and qualitatively inaccurate for application to smaller, lighter designs. 100 passenger narrow body transports, regional jets and executive aircraft. As the aircraft structure transitions from a strength dominated to a buckling dominated design, the impact of configuration changes upon structural weight changes dramatically. Buckling dominated aircraft wings are both disproportionately heavy, yet relatively insensitive to traditional configuration variables (sweep, *t/c* or *AR*). More importantly, the improvements in metallurgy that enable stronger alloys make wings more likely to be buckling dominated in detail design. We demonstrate here how the theoretical weight savings of a high strength alloys might prove to be illusory when applied to a smaller aircraft.

Acknowledgments

This manuscript derives from work Mr. Lemonds performed in partial fulfillment of the degree requirements for obtaining his M.S. in Aerospace Engineering from Arizona State University. All analysis on this unfunded project was completed at Arizona State University.

References

[1] Raymer, D. *Aircraft Design : A Conceptual Approach*, AIAA, 2006.
[2] Roskam, J., Airplane Design. Part V. Component Weight Estimation, DAR Corp, 1999.
[3] Nicolai, L., *Fundamentals of Aircraft Design*, METS, 1974.
[4] Torenbeek, E., "Prediction of Group Weight for Preliminary Design," Aircraft Engineering, pp. 16-21. July 1971.
[5] Torenbeek, E., *Synthesis of Subsonic Airplane Design*, Delft University Press, Delft, Holland, 1982
[6] McCullers, L.A., FLOPS: Aircraft Configuration Optimization. NASA CP-2327, 1984
[7] Takahashi, T.T. and Lemonds, T. "Transport Category Wing Weight Estimation Using A Optimizing Beam-Element Structural Formulation," AIAA 2015-#### (2015).
[8] Niu, M.C.Y., *Airframe Structural Design*, 2nd Ed, Hong Kong Conmilit Press Ltd, 1988.
[9] Niu, M.C.Y., *Airframe Stress Analysis and Sizing*, 2nd Ed. Hong Kong Conmilit Press Ltd., 1997.
[10] 14 CFR § 25.337 (2014). *Limit maneuvering load factors.* ("Except where limited by maximum (static) lift coefficients, the airplane is assumed to be subjected to symmetrical maneuvers resulting in the limit maneuvering load factors prescribed in this section. … The positive limit maneuvering load factor *n* … may not be less than 2.1+24,000/(W+10,000) except that *n* may not be less than 2.5 and need not be greater than … The negative limit maneuvering load factor … may not be less than −1.0")
[11] MIL HDBK 5-J
[12] 14 CFR § 25.303 (2014). *Factor of safety*. ("Unless otherwise specified, a factor of safety of 1.5 must be applied to the prescribed limit load which are considered external loads on the structure.")
[13] MSC Software. *Linear Static Analysis User's Guide: MSC Nastran 2012*, MSC Software, 2011.
[14] 14 CFR § 25.305 (2014). *Strength and Deformation.*